ACS APPLIED MATERIALS & INTERFACES

Research Article

www.acsami.org

One-Step Synthesis of Precursor Oligomers for Organic Photovoltaics: A Comparative Study between Polymers and Small Molecules

Wei Li,[†,‡,§] Daojuan Wang,[†,⊥] Suhao Wang,[∥] Wei Ma,[*,#] Svante Hedström,[□] David Ian James,[‡] Xiaofeng Xu,[‡] Petter Persson,[□] Simone Fabiano,[∥] Magnus Berggren,[∥] Olle Inganäs,[⊥] Fei Huang,[*,§] and Ergang Wang[*,‡]

[‡]Department of Chemistry and Chemical Engineering, Chalmers University of Technology, SE-41296 Göteborg, Sweden

[§]Institute of Polymer Optoelectronic Materials and Devices, State Key Laboratory of Luminescent Materials and Devices, South China University of Technology, Guangzhou 510640, P. R. China

[⊥]Biomolecular and Organic Electronics, IFM, Linköping University, SE−58183 Linköping, Sweden

[∥]Laboratory of Organic Electronics, Department of Science and Technology, Linköping University, SE−60174 Norrköping, Sweden

[#]State Key Laboratory for Mechanical Behavior of Materials, Xi'an Jiaotong University, Xi'an 710049, China

[□]Division of Theoretical Chemistry, Lund University, SE−221 00 Lund, Sweden

Supporting Information

ABSTRACT: Two series of oligomers TQ and rhodanine end-capped TQ-DR were synthesized using a facile one-step method. Their optical, electrical, and thermal properties and photovoltaic performances were systematically investigated and compared. The TQ series of oligomers were found to be amorphous, whereas the TQ-DR series are semicrystalline. For the TQ oligomers, the results obtained in solar cells show that as the chain length of the oligomers increases, an increase in power conversion efficiency (PCE) is obtained. However, when introducing 3-ethylrhodanine into the TQ oligomers as end groups, the PCE of the TQ-DR series of oligomers decreases as the chain length increases. Moreover, the TQ-DR series of oligomers give much higher performances compared to the original amorphous TQ series of oligomers owing to the improved extinction coefficient (ε) and crystallinity afforded by the rhodanine. In particular, the highly crystalline oligomer TQ5-DR, which has the shortest conjugation length shows a high hole mobility of 0.034 $cm^2 V^{-1} s^{-1}$ and a high PCE of 3.14%, which is the highest efficiency out of all of the six oligomers. The structure−property correlations for all of the oligomers and the TQ1 polymer demonstrate that structural control of enhanced intermolecular interactions and crystallinity is a key for small molecules/oligomers to achieve high mobilities, which is an essential requirement for use in OPVs.

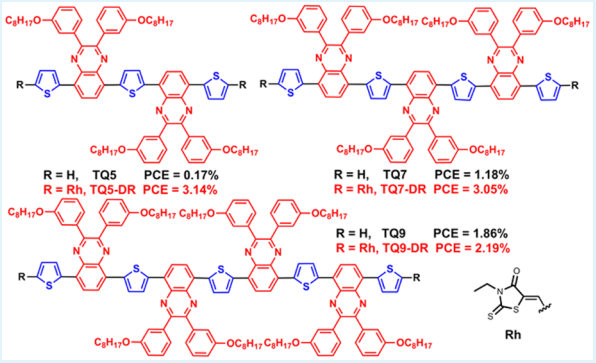

KEYWORDS: *crystallinity, amorphous, one-step method, oligomers, hole mobility, organic photovoltaics*

INTRODUCTION

Organic photovoltaics (OPVs) are regarded as a promising next-generation green technology for power generation with several advantages such as being lightweight, low cost, and flexible.[1−5] The most efficient OPVs are based on the bulk heterojunction concept, where an electron donor material is intimately mixed with an electron acceptor material to provide a large-area donor−acceptor interface. This aids charge separation and the formation of bicontinuous interpenetrating networks for charge transport.[6,7] Intensive efforts have been focused on the development of new donor materials with the aim of extending their absorption spectra, fine-tuning their energy levels and enhancing their mobilities. An effective and well-studied synthetic strategy to achieve such properties is to incorporate electron donating (D) and accepting (A) moieties in an alternating manner.[8−14] Both polymers and small molecules have been developed using this strategy and used as donor materials for OPVs achieving PCEs of around 10%.[15,16] There are several advantages and disadvantages of using either polymers or small molecules.[3,17−22] On the one hand, polymers have the advantages of ease of synthesis, good film-forming properties, and flexibility relative to small molecules, but suffer from large batch-to-batch variations, difficulty in purification, and wide molecular weight distribu-

Received: July 20, 2015
Accepted: November 23, 2015

DOI: 10.1021/acsami.5b09460
ACS Appl. Mater. Interfaces XXXX, XXX, XXX−XXX

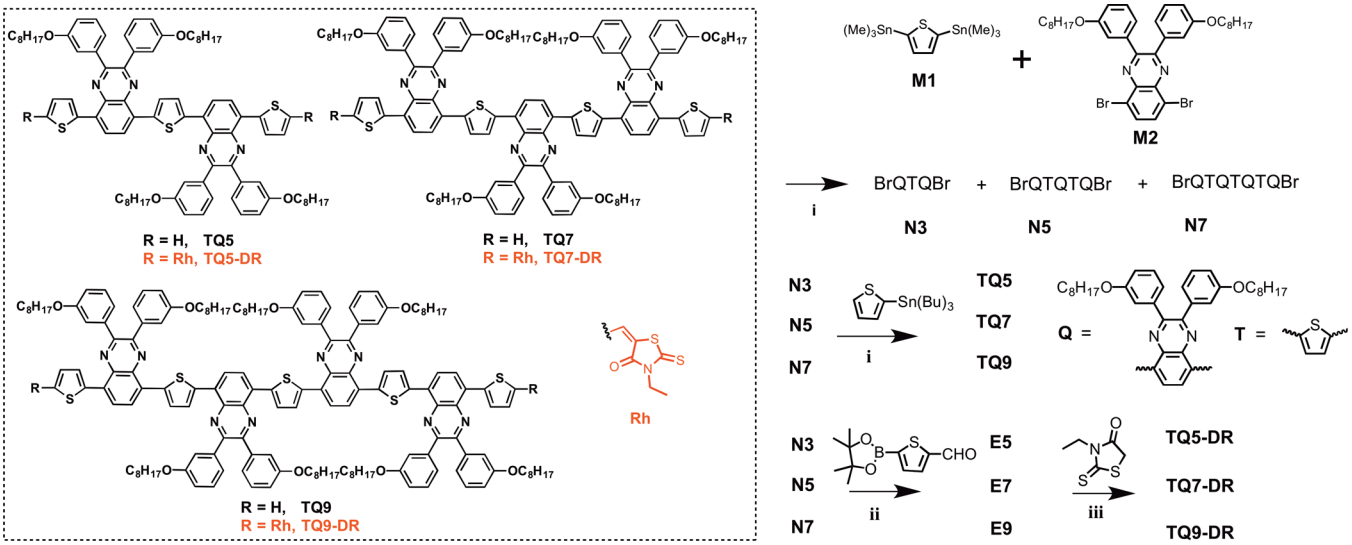

Figure 1. Structure and synthesis of the oligomers. (i) $Pd_2(dba_2)_3$, P(*o*-tol)$_3$, Toluene, 100 °C, 3 h; (ii) $Pd_2(dba)_3$, P(*o*-tol)$_3$, toluene, A336, K_3PO_4, H_2O, 95 °C, 12−24 h; (iii) piperidine, $CHCl_3$, reflux, 24 h.

tions. On the other hand, small molecules have reduced batch-to-batch variation, ease of purification, and are composed of defined structures without molecular weight distributions. However, there is a lack of a systematic and comparative study between polymers and small molecules composed of similar units, which would give a clearer picture of the structure−property relationships involved in OPV devices.

A survey of the literature indicates that most high-performing small molecules are highly crystalline[16,23−26] and that little attention has been given to the use of amorphous small molecules. Therefore, a comparative study between crystalline and amorphous small molecules with similar structures should be of interest. In our previous studies, an easily synthesized D−A polymer poly[2,3-bis(3-octyloxyphenyl)quinoxaline-5,8-diyl-*alt*-thiophene-2,5-diyl](TQ1) has been developed and shows promising performance with PCEs of 6−7% in solar cells,[27,28] despite the fact that TQ1 is largely amorphous.[29,30] Therefore, TQ oligomers were selected and synthesized for a comparative study with the amorphous polymer TQ1.

In this context, we report on the synthesis of a series of well-defined oligomers based on TQ units. The normal synthetic methods for synthesizing oligomers are quite lengthy and time-consuming, involving the extension of small molecules in a step-by-step process.[16,25,31,32] Here we propose a facile way to synthesize a series of oligomers using a one-step method. Although a one-step method has the obvious advantage of saving synthetic effort, it has been rarely used for the synthesis of conjugated materials for organic electronics. By judiciously choosing the stoichiometry of two monomers 2,5-bis-(trimethylstannyl)thiophene (M1) and 5,8-dibromo-2,3-bis(3-(octyloxy)phenyl)quinoxaline (M2), a series of oligomers were synthesized in one-step, which could be readily separated using normal silica gel column chromatography. Rhodanine as a popular end group for small molecules was introduced to the TQ oligomers as the end groups to give TQ-DR, which were compared with the amorphous TQ oligomers. The chemical structures are shown in Figure 1. The chain-length dependence of the thermal, optical, electrochemical and structural properties of the oligomers has been investigated both in solution and in the solid state. These oligomers have been used as the donor material for the fabrication of solution-processed BHJ cells with [6,6]-phenyl-C_{71}-butyric acid methyl ester ($PC_{71}BM$) as the electron acceptor and the results obtained have been used to deduce structure−property relationships.

RESULTS AND DISCUSSION

Design and Synthesis of Oligomers. Initially a series of precursors of the oligomers were synthesized using a one-step Stille coupling reaction (Figure 1). The reaction was carried out by initially dissolving the catalyst in toluene and an excess amount of the more stable dibromo-monomer M2. The ditin monomer M1 was added dropwise over the course of 6 h until an optimized M1:M2 ratio of 1:2 was obtained. The slow dropwise addition of tin monomer M1 ensured that the concentration of M1 was low to avoid the formation of high-molecular-weight polymers. As expected a series of precursor oligomers with repeating unit numbers between 2−4 formed with bromine remaining at each end of the precursor oligomers owing to the use of an excess of the M2 monomer. This allowed for further functionalization of the precursors. The precursors N3, N5 and N7 were obtained in the yield of 14.7, 12.1, and 16.4%, respectively. After purification and separation of the precursors by column chromatography, tributyl-(thiophen-2-yl)stannane was used to end-cap the precursors yielding the oligomers TQ5, TQ7, and TQ9. Further functionalization of the precursors via coupling with 5-(4,4,5,5-tetramethyl-1,3,2-dioxaborolan-2-yl)thiophene-2-carbaldehyde and then 3-ethylrhodanine yielded the other series of oligomers TQ5-DR, TQ7-DR and TQ9-DR with rhodanine end groups. The chemical structure of all of the final molecules was confirmed through ^{1}H and ^{13}C NMR spectroscopy and MALDI-TOF. Detailed reaction procedures and characterization of all the compounds can be found in the Supporting Information.

Thermal Properties. Solid-state thermal transitions were evaluated by using differential scanning calorimetry (DSC) under N_2 at a heating/cooling rate of 10 °C/min. The results of this study are shown in Figure 2. The melting temperatures-(T_m) and crystallization temperatures (T_c), together with the changes of relevant enthalpies (ΔH_m and ΔH_c) are summarized in Table 1. A high T_m of 227 and 236 °C and T_c of 221 and 229 °C were observed for TQ7-DR and TQ9-DR, respectively.

DOI: 10.1021/acsami.5b09460
ACS Appl. Mater. Interfaces XXXX, XXX, XXX−XXX

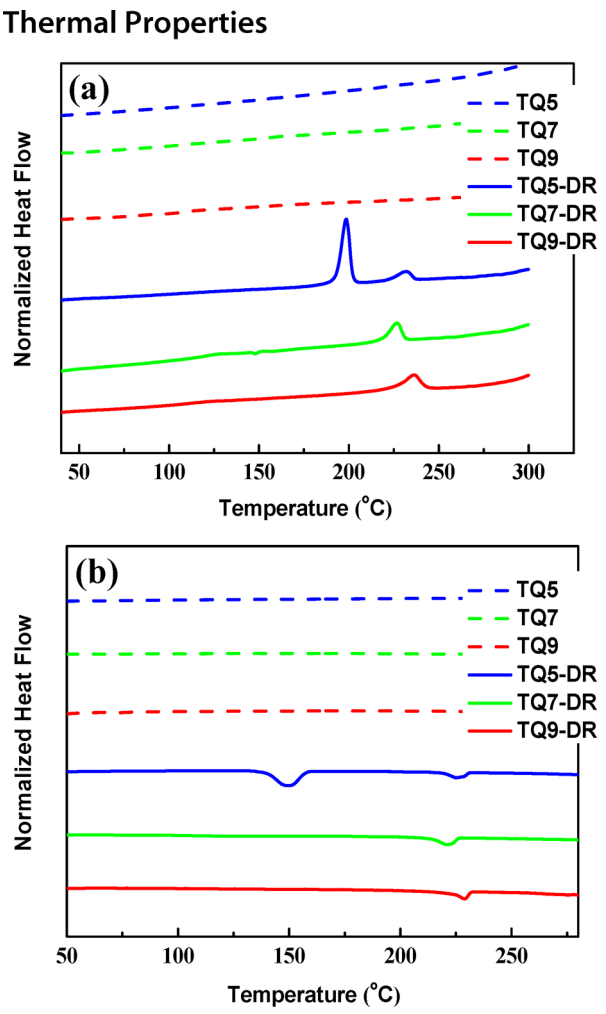

Figure 2. (a) Heating and (b) cooling DSC traces of the molecules.

Table 1. MS and DSC Properties of the Oligomers

molecules	MS_{calc} (m/z)	MS_{TOF}[a] (m/z)	T_m (°C)	T_c (°C)	ΔH_m (J/g)	ΔH_c (J/g)
TQ5	1320.7	1320.0				
TQ7	1938.9	1938.5				
TQ9	2557.3	2557.7				
TQ5-DR	1662.6	1662.7	205, 241	152, 235	18.9, 4.2	15.9, 3.7
TQ7-DR	2280.9	2280.2	227	221	7.4	5.5
TQ9-DR	2899.3	2899.3	236	229	5.1	4.7

[a]MS_{TOF} molecular weights are measured via the MALDI-TOF measurements.

However, TQ5-DR exhibits two endothermic peaks at 205 and 241 °C upon heating and two exothermic peaks at 152 and 235 °C upon cooling. Meanwhile, increasing molecule size from TQ5-DR and TQ9-DR leads to an obvious decrease in both ΔH_m(~15 J/g) and ΔH_c (~14 J/g). The difference in crystallization behavior of TQ5-DR compared with TQ7-DR and TQ9-DR indicates that TQ5-DR shows greater crystallinity. In contrast, there are no visible thermal transitions for the TQ series of oligomers within the thermal range of the experiment. This indicates that the TQ series of oligomers are largely amorphous, which is consistent with the observation that the polymer TQ1 is also amorphous.[29]

Optical Properties. The UV−vis absorption spectra of the six oligomers in chloroform solution and thin films are shown in Figure 3, while the corresponding data are listed in Table S1.

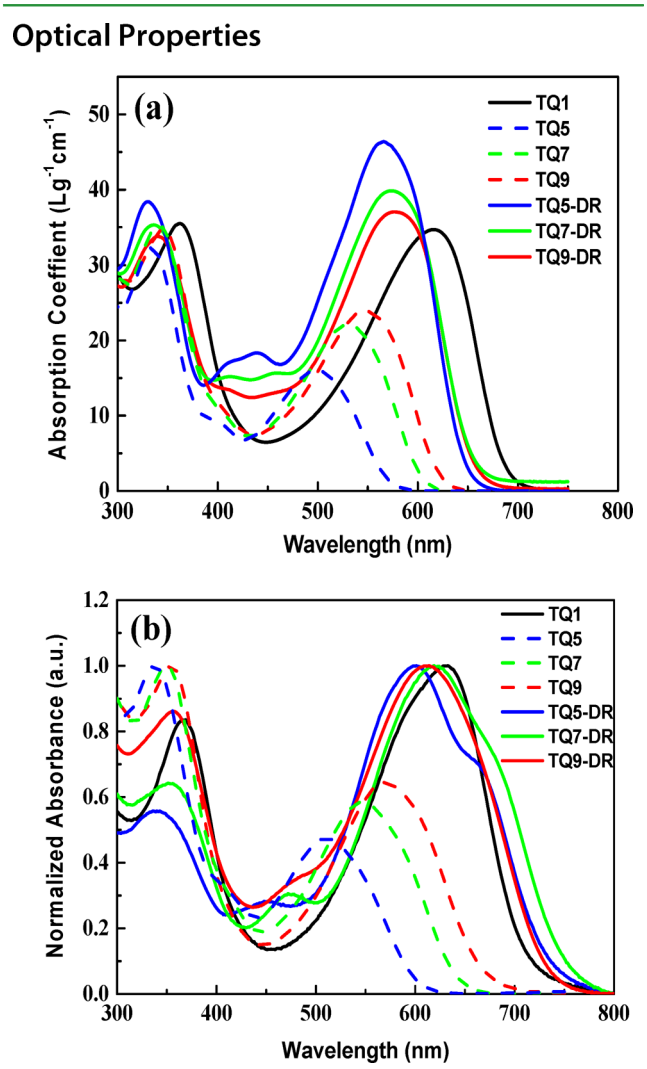

Figure 3. UV−vis absorption spectra of molecules (a) in chloroform solution and (b) in film.

For the TQ series of oligomers, chain extension leads to a progressive bathochromic shift of the absorption maximum (λ_{max}) with an increase in the absorption coefficients (ε) of the long wavelength absorption peaks. The absorption peaks at short wavelength originates from a $\pi-\pi^*$ transition with little or no associated intramolecular charge transfer (ICT), which is more or less independent of the chain length. The absorption bands at long wavelength from ICT transitions are however enhanced as the chains are elongated. Similar phenomena have also been observed in other oligomers.[31] However, for the TQ-DR series of oligomers with 3-ethylrhodanine as a terminal electron-withdrawing group, chain extension leads to almost no bathochromic shift of the λ_{max} with decrease of ε for the ICT peaks. The decrease of ε can be explained by the strong electron-withdrawing nature of 3-ethylrhodanine end groups and the decreased proportion of 3-ethylrhodanine along the increase of repeating units. It is noteworthy that the TQ-DR series of oligomers present a red shift of the λ_{max} and a higher ε compared to the corresponding TQ series of oligomers because of the effect of the 3-ethylrhodanine being a strong electron-

DOI: 10.1021/acsami.5b09460
ACS Appl. Mater. Interfaces XXXX, XXX, XXX−XXX

withdrawing group. Encouragingly, the ε of the TQ-DR series of oligomers is greater than that of the polymer TQ1, despite the fact that TQ1 shows a red-shifted λ_{max} (Figure 3), which can further confirm the contribution of 3-ethylrhodanine in the improvement of the ε.[33,34] As shown in Figure S1, the absorption spectra of the TQ-DR series of oligomers present a red-shift of their λ_{max} when going from solution to thin film and this red-shift is more pronounced than that of the TQ series of oligomers and the TQ1 polymer. This phenomenon indicates that the TQ-DR series of oligomers show strong aggregation or $\pi-\pi$ stacking between their molecular backbones. In particular, the TQ5-DR film cast from chloroform shows a λ_{max} at 601 nm along with a clear shoulder at 660 nm, which indicates that TQ5-DR has stronger aggregation or greater $\pi-\pi$ stacking between the molecular backbones compared to the other two TQ-DR oligomers TQ7-DR and TQ9-DR. This agrees well with the observation from DSC measurements that TQ5-DR shows greater crystallinity. From the Table S1 it can be seen that as the number of repeat units increases, the optical band gap of the TQ series of oligomers decreases dramatically, which is consistent with the same observation seen for other oligomers.[30] However, for the TQ-DR series of oligomers, all of the oligomers exhibit similar optical band gaps around 1.65 eV regardless of chain length, which can probably be attributed to the strong electron-withdrawing group 3-ethylrhodanine.

Cyclic Voltammetry. The highest occupied molecular orbital (HOMO) and lowest unoccupied molecular orbital (LUMO) energy levels were estimated using cyclic voltammetry (CV). Due to the greater solubility of these molecular materials relative to their polymeric counterparts, it is hard to estimate their energy levels from thin films, thus their energy levels were estimated via solution-based CV measurements. The HOMO and LUMO positions were derived from the onset of the oxidation (E_{ox}) and reduction potentials (E_{red}) from the CV curves (Figure S2). All of the potentials were calibrated with the standard ferrocene/ferrocenium redox couple. According to the equations HOMO = $-(E_{ox} + 5.13)$ eV and LUMO = $-(E_{red} + 5.13)$ eV,[35] the respective HOMO and LUMO energies (versus vacuum) were calculated and are summarized in Figure S3. As expected, the chain extension leads to a visible increase in the HOMO levels of the TQ oligomers, which are close to the HOMO level of the TQ1 polymer. The LUMO levels of TQ oligomers and TQ1 polymer are the same. It can be explained by that the HOMO levels of the TQ oligomers are more sensitive to the change of conjugated chain length compared to the LUMO levels, which is consistent with the theoretical results. On the other hand, for TQ-DR series, the end group 3-ethylrhodanine mainly determines the LUMO levels of the oligomers, while not affecting the HOMO levels, so chain extension leads to an obviously increase in the HOMO levels of the TQ-DR oligomers. However, the LUMO levels for TQ-DR oligomers remain unchanged as the conjugated chain length of the oligomers increases, which is inconsistent with the theoretical results. The detailed information can be found in the Theoretical Simulations section. The LUMO levels of the TQ-DR series of oligomers are 0.15 eV lower than that of the TQ series of oligomers due to the influence of the stronger electron-withdrawing group, 3-ethylrhodanine, whereas their HOMO levels are comparable to that of the TQ series of oligomers.

Theoretical Simulations. To further understand the optical and photophysical properties of the six oligomers investigated in this work, we carried out density functional theory (DFT) calculations using the ωB97XD/6-31G(d,p) exchange-correlation density functional and basis set.[36] This functional has been used before for the polymer TQ1,[37] and includes an empirical dispersion term, which is important for accurately describing the phenyl side group interactions. The oligomers then underwent TD-DFT calculations at the PBE0/6-31G(d,p) level of theory to obtain excited state data.[38] A Gaussian broadening of 3000 cm^{-1}, with an inhomogeneity factor of 1.5 was applied to the calculated transitions in order to simulate absorption spectra. Long alkyl side chains were truncated to shorter methyl or isopropyl groups in order to reduce computational time. The calculated absorption spectra in vacuum, the molecular geometries, the average out-of-plane dihedral angles, the frontier orbitals and the calculated HOMO, LUMO energy levels for all six molecules are depicted in Figure S4, Figure S5, Table S2, Figure 4, and Figure S3, respectively.

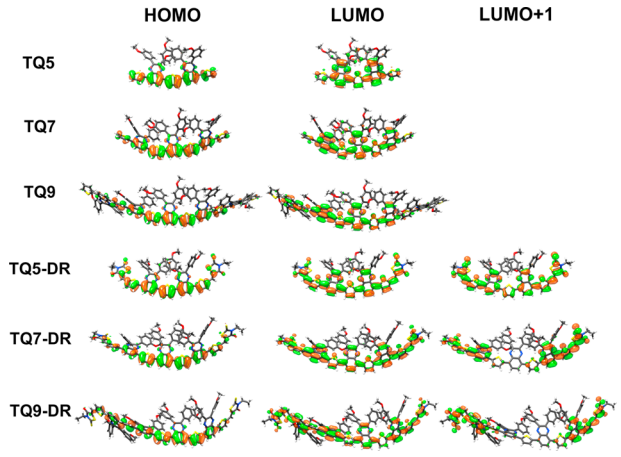

Figure 4. Calculated frontier orbitals of the oligomers (isovalue = 0.02).

From Figure S4, we can see that chain extension leads to a progressive bathochromic shift of the λ_{max} with an increase of the ε for the TQ series of oligomers and a small bathochromic shift of the λ_{max} with a decrease of the ε for the TQ-DR series of oligomers, which is consistent with the experimental results. Also the absolute λ_{max} and ε agree with experiments, although the somewhat too narrow arbitrary broadening leads to overestimated ε_{max}. As shown in Figure S4, for the TQ series of oligomers, the long wavelength absorption peak is a HOMO → LUMO CT-transition, analogous to that of the TQ1 polymer.[37] However, for the TQ-DR series of oligomers, the long wavelength absorption peak is due to a HOMO → LUMO transition, and becomes weaker with an increasing number of TQ units. This is because it corresponds to a CT transition from the TQ unit to the 3-ethylrhodanine, and as the number of TQ units increase, the spatial overlap between the TQ-centered HOMO and the rhodanine-localized LUMO becomes poorer (Figure 4). From Figure S3, it is apparent that the calculated orbital energies are consistently overestimated compared to the experimental values because of limitations in Koopman's theorem, e.g., the DFT produces nonrelaxed orbitals, which is common for conjugated polymers.[39] The HOMO energy level of both series of oligomers goes up as the number of TQ repeating units increase, which shows the same trend as the experimental results. However, the LUMO energy levels for the two oligomer series show different trends. The

DOI: 10.1021/acsami.5b09460
ACS Appl. Mater. Interfaces XXXX, XXX, XXX−XXX

TQ series of oligomers have almost constant LUMO energies, which is consistent with the experimental results. The TQ-DR series of oligomers, however, shows calculated LUMO energies that goes up with the number of TQ repeating units, because of the LUMOs becoming more localized on the two rhodanine groups as a result of the decreasing proportion of the end group 3-ethylrhodanine relative to the TQ unit (Figure 4). The different trends between the theoretical and experimental results for the LUMO energies of the TQ-DR series are not completely unexpected due to the virtual nature of calculated unoccupied orbitals,[40] but it may indicate that other mechanisms affect the LUMO energies in the TQ-DR series of oligomers. Unfortunately, as shown in Figure S5, all of these molecules exhibit a nonplanar structure due to the effect of the phenyl side groups. The out-of-plane dihedral angles for the TQ-DR series of oligomers are much smaller than that of the TQ series of oligomers due to the fact that the T-Rh is almost completely coplanar because of the absence of steric hindrance from colliding hydrogen atoms. Encouragingly, the TQ5-DR oligomer has the smallest dihedral angle (10.2°) out of all six oligomers, which indicates that TQ5-DR has the potential to form the strongest $\pi-\pi$ stacking interactions between neighboring chains out of all of the oligomers. This is consistent with the observations seen in the DSC measurements and absorption spectra.

Structural Investigations. To gain further insight into the molecular packing in thin films, we used grazing incident wide-angle X-ray scattering (GIWAXS). Out-of-plane line cuts were shown along with the 2D scattering profiles in Figure 5. The TQ5-DR pure film scattering pattern shows strong, diffraction peaks indicative of high crystallinity. The diffraction peaks were recorded in the out-of-plane (OOP) direction, to probe the structural order of the materials normal to the substrate. The (h00) diffraction peaks at $q = h0.30$ Å^{-1} for the TQ5-DR at the OOP direction, corresponds to a spacing of 20.9 Å. A strong (010) $\pi-\pi$ stacking is observed in the in-plane (IP) direction at q near 1.5−1.6 Å^{-1}, suggesting that the molecule adopts an edge-on orientation on the substrate for TQ5-DR. TQ9-DR diffractogram display an isotropic diffraction ring around 0.28 Å^{-1}, which can be assigned to the (100) spacing. Another ring around 1.5−1.6 Å^{-1} can be attributed to the $\pi-\pi$ stacking of TQ9-DR. The azimuthal distribution of the diffraction ring indicates a less preferred orientation of the crystallites inside the film. This model suggests that although TQ5-DR adopts an edge-on orientation with a high crystallinity, chain extension of the oligomers (TQ9-DR) leads to more disordered and amorphous material. The (010) $\pi-\pi$ stacking coherence length is calculated by the Scherrer equation. The coherence length for TQ5-DR and TQ9-DR is 50 and 28 Å. This further confirms that TQ5-DR shows better crystallinity.

Charge Carrier Mobilities. To investigate the charge transport properties of the oligomers, top-gate/bottom-contact organic field effect transistors (OFETs) were fabricated. The device fabrication procedure is described in the Supporting Information. All devices showed hole transport characteristics and the mobilities were calculated in the saturation regime (V_D = −80 V). The mobilities of the TQ series of oligomers were unable to be observed most likely due to the lack of $\pi-\pi$ stacking. For comparison, the charge transport characteristics of the polymer TQ1 were also investigated, which shows a saturation mobility of 0.0016 cm^2 V^{-1} s^{-1}. The TQ-DR series of oligomers however exhibit a comparably higher hole mobility (μ_h) than the TQ series on the order of 1×10^{-2} to 1×10^{-3} cm^2 V^{-1} s^{-1}, which is believed to be high enough for use in OPVs.[25,32,39] The transfer curves are plotted in Figure 6 and the related data are summarized in Table 2. Charge transport is believed to be more efficient along polymer chains and in the $\pi-\pi$ stacking direction. In the case of the TQ oligomers, their chains are very short (2−4 nm) meaning that there is little charge transport along the chains and as they are amorphous there is no $\pi-\pi$ stacking ordering resulting in no charge transport in the $\pi-\pi$ stacking direction thus giving an overall charge mobility that is extremely low. By comparison, the high-molecular-weight amorphous polymer TQ1 allows charge transport along the long polymer chain (20−30 nm), which results in a decent mobility being obtained. This is consistent with the same observation seen for other amorphous polymers. For the highly crystalline TQ-DR series of oligomers, it is possible for charges to be transported in the $\pi-\pi$ stacking direction and thus comparatively higher mobilities can be achieved. Moreover, the short oligomer TQ5-DR exhibits a higher mobility of 0.034 cm^2 V^{-1} s^{-1} than its longer analogues TQ7-DR and TQ9-DR, which can be explained by the most

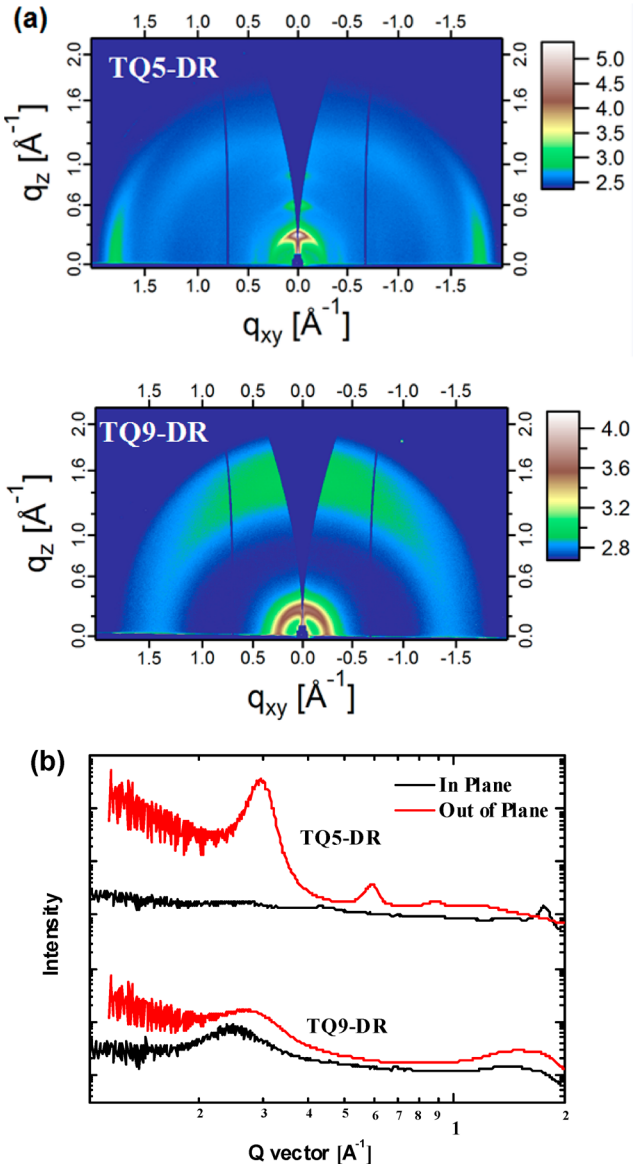

Figure 5. (a) 2D diffractograms and (b) out-of-plane line-cut profiles of thin films of TQ5-DR and TQ9-DR.

DOI: 10.1021/acsami.5b09460
ACS Appl. Mater. Interfaces XXXX, XXX, XXX−XXX

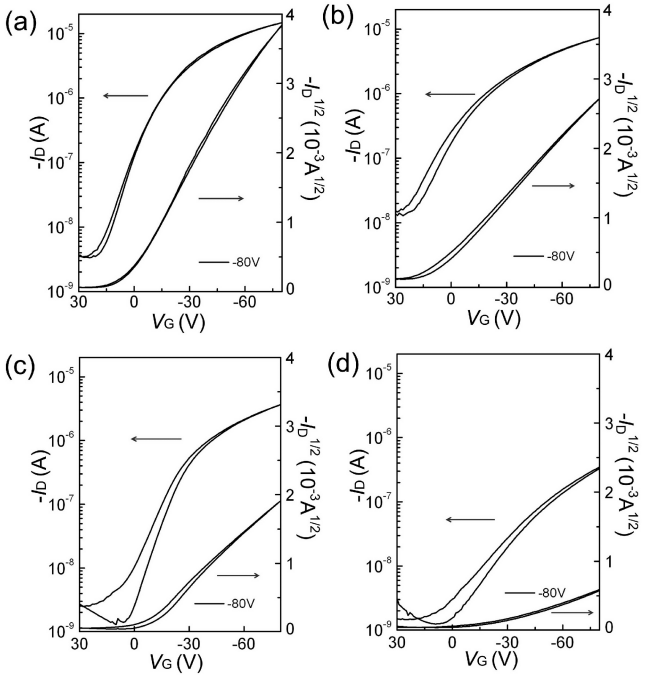

Figure 6. Typical transfer curves of OFET devices corresponding to (a) TQ5-DR, (b) TQ7-DR, (c) TQ9-DR, and (d) TQ1.

crystalline oligomer TQ5-DR as indicated by the absorption spectra, DSC and GIWAXS measurements. From this observation, we can further conclude that having high crystallinity is indispensable for small molecules to achieve high mobilities, which is an essential requirement for application in OPVs. We have to point out that the mobilities obtained from FETs are not the best ones to be correlated with OPV results; however, the data can be used to make a relative comparison in all oligomers and the TQ1 polymer.

Photovoltaic Characteristics. Solution-processed BHJ devices were fabricated using the six oligomers as the electron donor with a conventional device structure of ITO/PEDOT:PSS/Oligomers:$PC_{71}BM$/LiF/Al. The film thicknesses of the active layers and oligomer:$PC_{71}BM$ (D:A) ratio were optimized. We initially used chloroform as the processing solvent for the active layers. The related photovoltaic performance data and the characteristic current density–voltage (J–V) curves are shown in Table S3 and Figure S6. All of the devices give quite low performances with the best PCE of 1.78% being obtained for TQ5-DR. We noticed that the V_{oc} of TQ5 is quite low relative to its deeper HOMO level, which is probably due to its poor film quality leading to underestimated V_{oc}.

Considering the effect of the processing solvent on the morphology and photovoltaic performances of the BHJ devices, we then used *o*-dichlorobenzene (ODCB) as the processing solvent for the active layer to optimize the BHJ devices. However, because of the poor film quality for TQ5-DR and TQ9-DR processed by ODCB, the mixed solvent (chloroform:ODCB = 1:1) was used instead. The corresponding optimized device parameters together with the characteristic current density–voltage (J–V) curves for the optimized devices are summarized in Table 2 and Figure 7. Because of the poor film quality from ODCB or the mixed solvent system, TQ5 can obtain only a low device performance of 0.17% in devices processed from chloroform. From Table 2, we can see that chain extension of the TQ series of oligomers leads to an increase in J_{sc} from 0.79 mA cm^{-2} for TQ5 to 6.28 mA cm^{-2} for TQ9. Combined with a gradual increase in fill factor (FF) from 0.26 to 0.37, an increase of PCE from 0.17% to 1.86% was also observed. Similar phenomena have also been reported for other

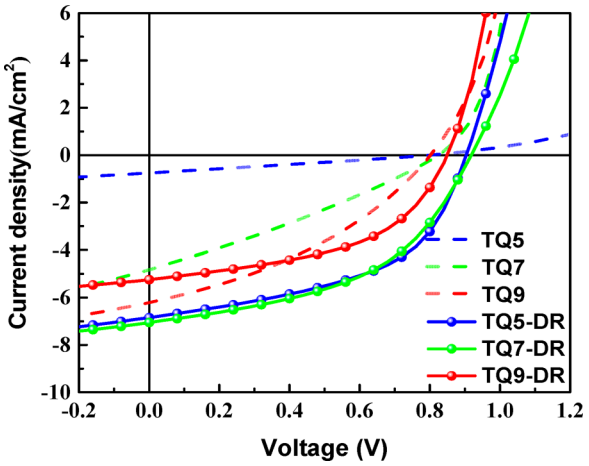

Figure 7. Characteristic current density vs voltage (J–V) curves for the optimized devices under simulated AM 1.5 G irradiation (100 mW cm^{-2}).

Table 2. Best Photovoltaic Performance of BHJ Solar Cells Based on Oligomers:$PC_{71}BM$ under the Optimized Conditions under Illumination of AM 1.5 G, 100 mW cm^{-2} and the Hole Mobility of the Oligomers and TQ1 Polymer Estimated by OFET Device

molecule	ratio D:A	FF	J_{sc} (mA cm^{-2})	V_{oc} (V)	PCE (%)	μ_h [e] average (cm^2 V^{-1} S^{-1})	μ_h [f] maximum (cm^2 V^{-1} S^{-1})
TQ5[a]	1:2	0.26	0.79	0.83	0.17		
TQ7[b]	1:2	0.29	4.89	0.83	1.18		
TQ9[b]	1:2	0.37	6.28	0.81	1.86		
TQ5-DR[c]	1:1	0.51	6.85	0.90	3.14	$1.5 \pm 1.1 \times 10^{-2}$	3.4×10^{-2}
TQ5-DR[d]	1:1	0.49	6.02	0.96	2.83		
TQ7-DR[b]	3:2	0.47	7.05	0.92	3.05	$9.1 \pm 1.0 \times 10^{-3}$	1.1×10^{-2}
TQ9-DR[c]	1:1	0.49	5.25	0.85	2.19	$8.3 \pm 1.5 \times 10^{-3}$	9.7×10^{-3}
TQ1[f]						$1.3 \pm 0.2 \times 10^{-3}$	1.6×10^{-3}

[a]Processed with chloroform without thermal annealing. [b]Processed with ODCB without thermal annealing. [c]Processed with mix solvent (chloroform:ODCB = 1:1) with TA at 120 °C for 10 min. [d]Processed with the mixed solvent (chloroform:ODCB = 1:1) without thermal annealing. [e]The FET mobilities were calculated in the saturation regime (V_D = −80 V). [f]The FET mobilities were calculated in the saturation regime (V_D = −80 V).

DOI: 10.1021/acsami.5b09460
ACS Appl. Mater. Interfaces XXXX, XXX, XXX–XXX

series of oligomers.[31] We tentatively attribute this increase in PCE to an increase in ε and the extended absorption spectra.

In contrast, a different trend was observed for the TQ-DR series of oligomers. As the conjugation length increased from TQ5-DR to TQ9-DR, the PCE decreased from 3.14 to 2.19%. It can be observed that both the J_{sc} and the FF of the TQ5-DR based devices are higher than that of the TQ9-DR based devices, which can be partially ascribed to its much higher absorption coefficient and the fact that the TQ5-DR has the greatest crystallinity, which enables higher mobilities.

Encouragingly, by comparing the performance of the TQ-DR series with the TQ series, we find that the strong electron-withdrawing group, 3-ethylrhodanine, enables higher device performances in OPVs to be obtained. This can be explained by the enhanced absorption coefficients and higher crystallinity and mobility observed in the TQ-DR series. To further confirm the higher hole mobility of TQ5-DR compared to TQ9, we studied the effect of film thickness on device performance based on the two aforementioned oligomers. The corresponding optimized device parameters together with the characteristic current density–voltage (J–V) curves are summarized in Table S4 and Figures S7 and Figure S8. As shown in Table S4, the PCE of TQ5-DR is not sensitive to the film thickness in the range of 90—140 nm; however, the PCE of TQ9 decreases very quickly when the film thickness increases from 90 to 110 nm. It is evident that the stronger crystallinity of TQ5-DR is a key factor that leads to higher hole-mobility, extended light-harvesting properties and thus higher photovoltaic performance.

The external quantum efficiency (EQE) curves of the optimized devices based on all of the oligomers are shown in Figure 8 (except of the device based on TQ5, which shows an

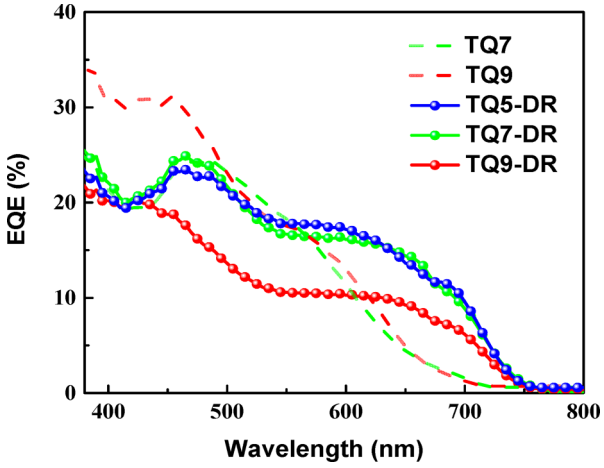

Figure 8. External quantum efficiency (EQE) curves for the optimized devices.

especially low J_{sc}). The spectra of the cells based on the TQ-DR oligomers show a broader response extending from 400 to 750 nm compared to those of the TQ series of oligomers. From the absorption and EQE profiles, the light harvesting contribution of $PC_{71}BM$ can be clearly seen, especially for the TQ series. The EQE values for the TQ9 based device are distinctly higher than that of TQ5-DR from 400 to 500 nm owing to the higher contribution of $PC_{71}BM$ in the TQ9 device (D:A = 1:2) to the photocurrent, and the EQE curve for the device based on TQ5-DR exhibits a stronger response from 600 to 750 nm due to the strong absorption of TQ5-DR in this region. As a result, the device based on TQ5-DR shows a comparable J_{sc} to that of TQ9. In addition, the currents obtained from the integral of the EQEs are consistent with the J_{sc} values from J–V curves.

Morphology Characterization. To understand the reasons for the influence of the processing solvents on the photovoltaic performance of the oligomers, we investigated the surface morphologies of the active layers using atomic force microscopy (AFM). The corresponding images in chloroform and in optimal solvents are shown in Figure S9 and Figure 9,

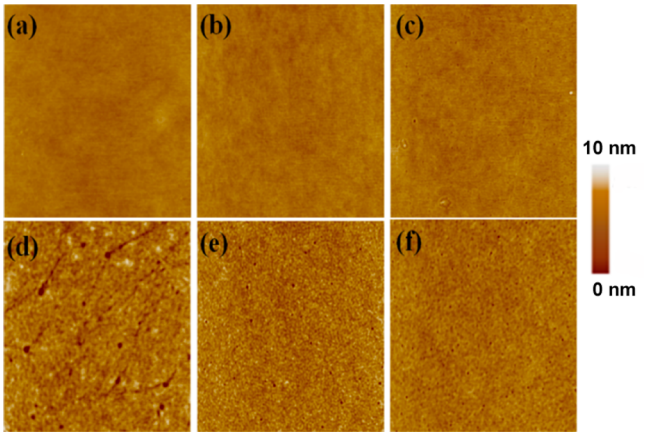

Figure 9. AFM topography images (5 × 5 μm^2) of blend films cast from optimal solvent: (a) TQ5, the RMS roughness 0.41 nm ($CHCl_3$). (b) TQ7, the RMS roughness 0.42 nm (ODCB). (c) TQ9, the RMS roughness 0.45 nm (ODCB). (d) TQ5-DR, the RMS roughness 1.19 nm. (ODCB:$CHCl_3$ = 1:1). (e) TQ7-DR, the RMS roughness 0.76 nm (ODCB). (f) TQ9-DR, the RMS roughness 0.56 nm (ODCB:$CHCl_3$ = 1:1).

respectively. The surface of the blend films based on the TQ-DR series processed from ODCB or mixed solvent system (chloroform:ODCB = 1:1) is smoother than that processed from just chloroform. As shown in Figure S9d–f, large domains form when the TQ-DR oligomers are processed with chloroform probably due to their high crystallinity. These large domains are indications of large phase separation, which is unfavorable for exciton diffusion and separation. All of the films show smooth surfaces without large domains when processed with the optimized solvent conditions and the root means roughness (RMS) values are summarized in Figure 9. This explains their improved performance when processed from ODCB or mixed solvents as summarized in Table 2. Although the surface of the films from the TQ series of oligomers are very smooth, the lack of π–π stacking to afford continuous percolating pathways for charge transport to the electrodes may be responsible for the low FF values obtained and consequently the low PCEs. On the other hand, the relatively rough surface of the film of TQ5-DR/$PC_{71}BM$ with a few randomly oriented fibrous structures may increase the heterojunction area and afford continuous networks. This is beneficial for exciton dissociation and charge transport, which in turn leads to a high J_{sc} and FF.[41−43] This is consistent with the high hole mobility of TQ5-DR seen in OFETs and the fact that it shows the highest crystallinity in GIWAXS and DSC measurements.

CONCLUSION

Two different series of oligomers TQ and rhodanine end-capped TQ-DR were synthesized using a facile one-step

DOI: 10.1021/acsami.5b09460
ACS Appl. Mater. Interfaces XXXX, XXX, XXX−XXX

method. The TQ series of oligomers were found to be amorphous while the introduction of rhodanine was found to be able to increase the crystallinity of the resulting TQ-DR series of oligomers. Conjugation length has a different impact on the optical properties and the device performance for the two series of oligomers. For the TQ series of oligomers, the results obtained in BHJ solar cells show that elongation of the chains leads to an increase in PCE. However, when introducing 3-ethylrhodanine into the TQ series of oligomers as end groups, the PCEs of the TQ-DR series of oligomers decreases as the chain length increases. Moreover, the TQ-DR series of oligomers give much higher performances compared to the original amorphous TQ series of oligomers because of the contribution of rhodanine in improving the ϵ and crystallinity. In particular, the highly crystalline oligomer TQ5-DR with the shortest conjugation length shows the highest hole mobility of 0.034 $cm^{-2}V^{-1}$ s^{-1} and the highest PCE of 3.14%. The low performance of the TQ series of oligomers can be attributed to their amorphous state in films and their short molecular chains, which limit the formation of continuous pathways for charge transport. For the TQ-DR series of oligomers, the high crystallinity induced by rhodanine makes it possible to form continuous networks through $\pi-\pi$ stacking interactions enabling charge transport. This coupled with an enhanced absorption coefficient, leads to an improved photovoltaic performance and hole mobility. This work discloses an important guideline for the design of small molecules/oligomers for OPVs. They should be highly crystalline so that continuous pathways for charge transport can form along the $\pi-\pi$ stacking direction. In the case of polymers, it is not necessary for them to be crystalline because amorphous polymers can also transport charges along their long polymer backbones.

■ ASSOCIATED CONTENT

Supporting Information

The Supporting Information is available free of charge on the ACS Publications website at DOI: 10.1021/acsami.5b09460.

Detailed synthetic procedures and characterization data for the new compounds and additional experimental results (PDF)

■ AUTHOR INFORMATION

Corresponding Authors

*E-mail: msewma@mail.xjtu.edu.cn.
*E-mail: msfhuang@scut.edu.cn.
*E-mail: ergang@chalmers.se.

Author Contributions

†W.L. and D.W. contributed equally.

Notes

The authors declare no competing financial interest.

■ ACKNOWLEDGMENTS

We thank the financial support from the Swedish Research Council and the Swedish Energy Agency as well as the Knut and Alice Wallenberg foundation for a Wallenberg Scholar grant to OI. WL and DW thank the China Scholarship Council for financial support. EW acknowledges the program for the Excellent Doctoral Dissertations of Guangdong Province (ybzzxm201114). FH acknowledges the Ministry of Science and Technology (No. 2014CB643501), the Natural Science Foundation of China (Nos. 21125419 and 51361165301) and Guangdong Natural Science Foundation (Grant No. S2012030006232). WL appreciates M. G. Andersson for his help with the DSC measurements. X-ray data was acquired at beamlines 7.3.3[44] and at the Advanced Light Source, which is supported by the Director, Office of Science, Office of Basic Energy Sciences, of the U.S. Department of Energy under Contract No. DE−AC02−05CH11231.

■ REFERENCES

(1) Zhou, H.; Yang, L.; You, W. Rational Design of High Performance Conjugated Polymers for Organic Solar Cells. *Macromolecules* **2012**, *45*, 607−632.
(2) Mishra, A.; Bäuerle, P. Small Molecule Organic Semiconductors on the Move: Promises for Future Solar Energy Technology. *Angew. Chem., Int. Ed.* **2012**, *51*, 2020−2067.
(3) Cheng, Y.-J.; Yang, S.-H.; Hsu, C.-S. Synthesis of Conjugated Polymers for Organic Solar Cell Applications. *Chem. Rev.* **2009**, *109*, 5868−5923.
(4) Thompson, B. C.; Fréchet, J. M. J. Polymer−Fullerene Composite Solar Cells. *Angew. Chem., Int. Ed.* **2008**, *47*, 58−77.
(5) Lin, Y.; Li, Y.; Zhan, X. Small Molecule Semiconductors for High-efficiency Organic Photovoltaics. *Chem. Soc. Rev.* **2012**, *41*, 4245−4272.
(6) Günes, S.; Neugebauer, H.; Sariciftci, N. S. Conjugated Polymer-Based Organic Solar Cells. *Chem. Rev.* **2007**, *107*, 1324−1338.
(7) Yu, G.; Gao, J.; Hummelen, J. C.; Wudl, F.; Heeger, A. J. Polymer Photovoltaic Cells: Enhanced Efficiencies via a Network of Internal Donor-Acceptor Heterojunctions. *Science* **1995**, *270*, 1789−1791.
(8) Blouin, N.; Michaud, A.; Gendron, D.; Wakim, S.; Blair, E.; Neagu-Plesu, R.; Belletête, M.; Durocher, G.; Tao, Y.; Leclerc, M. Toward a Rational Design of Poly(2,7-Carbazole) Derivatives for Solar Cells. *J. Am. Chem. Soc.* **2008**, *130*, 732−742.
(9) Li, Y. Molecular Design of Photovoltaic Materials for Polymer Solar Cells: Toward Suitable Electronic Energy Levels and Broad Absorption. *Acc. Chem. Res.* **2012**, *45*, 723−733.
(10) Wang, E.; Mammo, W.; Andersson, M. R. 25th Anniversary Article: Isoindigo-Based Polymers and Small Molecules for Bulk Heterojunction Solar Cells and Field Effect Transistors. *Adv. Mater.* **2014**, *26*, 1801−1826.
(11) Dang, D. F.; Chen, W. C.; Himmelberger, S.; Tao, Q.; Lundin, A.; Yang, R. Q.; Zhu, W. G.; Salleo, A.; Müller, C.; Wang, E. Enhanced Photovoltaic Performance of Indacenodithiophene-Quinoxaline Co-polymers by Side-Chain Modulation. *Adv. Energy Mater.* **2014**, *4*, 1400680.
(12) Ma, Z. F.; Dang, D. F.; Tang, Z.; Gedefaw, D.; Bergqvist, J.; Zhu, W. G.; Mammo, W.; Andersson, M. R.; Inganäs, O.; Zhang, F. L.; Wang, E. G. A Facile Method to Enhance Photovoltaic Performance of Benzodithiophene-Isoindigo Polymers by Inserting Bithiophene Spacer. *Adv. Energy Mater.* **2014**, *4*, 1301455.
(13) Biniek, L.; Schroeder, B. C.; Nielsen, C. B.; McCulloch, I. Recent Advances in High Mobility Donor-acceptor Semiconducting Polymers. *J. Mater. Chem.* **2012**, *22*, 14803−14813.
(14) Ma, Z.; Sun, W.; Himmelberger, S.; Vandewal, K.; Tang, Z.; Bergqvist, J.; Salleo, A.; Andreasen, J. W.; Inganäs, O.; Andersson, M. R.; Muller, C.; Zhang, F.; Wang, E. Structure-property Relationships of Oligothiophene-isoindigo Polymers for Efficient Bulk-heterojunction Solar Cells. *Energy Environ. Sci.* **2014**, *7*, 361−369.
(15) Liu, Y.; Zhao, J.; Li, Z.; Mu, C.; Ma, W.; Hu, H.; Jiang, K.; Lin, H.; Ade, H.; Yan, H. Aggregation and Morphology Control Enables Multiple Cases of High-efficiency Polymer Solar Cells. *Nat. Commun.* **2014**, *5*, 5293.
(16) Kan, B.; Li, M.; Zhang, Q.; Liu, F.; Wan, X.; Wang, Y.; Ni, W.; Long, G.; Yang, X.; Feng, H.; Zuo, Y.; Zhang, M.; Huang, F.; Cao, Y.; Russell, T. P.; Chen, Y. A Series of Simple Oligomer-like Small Molecules Based on Oligothiophenes for Solution-Processed Solar Cells with High Efficiency. *J. Am. Chem. Soc.* **2015**, *137*, 3886−3893.

DOI: 10.1021/acsami.5b09460
ACS Appl. Mater. Interfaces XXXX, XXX, XXX−XXX

(17) Roncali, J.; Leriche, P.; Blanchard, P. Molecular Materials for Organic Photovoltaics: Small is Beautiful. *Adv. Mater.* **2014**, *26*, 3821−3838.
(18) Li, W.; Yang, L.; Tumbleston, J. R.; Yan, L.; Ade, H.; You, W. Controlling Molecular Weight of a High Efficiency Donor-Acceptor Conjugated Polymer and Understanding Its Significant Impact on Photovoltaic Properties. *Adv. Mater.* **2014**, *26*, 4456−4462.
(19) Chen, J.; Cao, Y. Development of Novel Conjugated Donor Polymers for High-Efficiency Bulk-Heterojunction Photovoltaic Devices. *Acc. Chem. Res.* **2009**, *42*, 1709−1718.
(20) Svensson, M.; Zhang, F.; Veenstra, S. C.; Verhees, W. J. H.; Hummelen, J. C.; Kroon, J. M.; Inganäs, O.; Andersson, M. R. High-Performance Polymer Solar Cells of an Alternating Polyfluorene Copolymer and a Fullerene Derivative. *Adv. Mater.* **2003**, *15*, 988−991.
(21) Wang, E.; Wang, L.; Lan, L.; Luo, C.; Zhuang, W.; Peng, J.; Cao, Y. High-performance Polymer Heterojunction Solar Cells of A Polysilafluorene Derivative. *Appl. Phys. Lett.* **2008**, *92*, 033307.
(22) Henson, Z. B.; Müllen, K.; Bazan, G. C. Design Strategies for Organic Semiconductors beyond the Molecular Formula. *Nat. Chem.* **2012**, *4*, 699−704.
(23) Kan, B.; Zhang, Q.; Li, M.; Wan, X.; Ni, W.; Long, G.; Wang, Y.; Yang, X.; Feng, H.; Chen, Y. Solution-Processed Organic Solar Cells Based on Dialkylthiol-Substituted Benzodithiophene Unit with Efficiency near 10%. *J. Am. Chem. Soc.* **2014**, *136*, 15529−15532.
(24) Zhou, J.; Zuo, Y.; Wan, X.; Long, G.; Zhang, Q.; Ni, W.; Liu, Y.; Li, Z.; He, G.; Li, C.; Kan, B.; Li, M.; Chen, Y. Solution-Processed and High-Performance Organic Solar Cells Using Small Molecules with a Benzodithiophene Unit. *J. Am. Chem. Soc.* **2013**, *135*, 8484−8487.
(25) Liu, X.; Sun, Y.; Hsu, B. B. Y.; Lorbach, A.; Qi, L.; Heeger, A. J.; Bazan, G. C. Design and Properties of Intermediate-Sized Narrow Band-Gap Conjugated Molecules Relevant to Solution-Processed Organic Solar Cells. *J. Am. Chem. Soc.* **2014**, *136*, 5697−5708.
(26) Sun, Y.; Welch, G. C.; Leong, W. L.; Takacs, C. J.; Bazan, G. C.; Heeger, A. J. Solution-Processed Small-molecule Solar Cells with 6.7% Efficiency. *Nat. Mater.* **2012**, *11*, 44−48.
(27) Wang, E.; Hou, L.; Wang, Z.; Hellström, S.; Zhang, F.; Inganäs, O.; Andersson, M. R. An Easily Synthesized Blue Polymer for High-Performance Polymer Solar Cells. *Adv. Mater.* **2010**, *22*, 5240−5244.
(28) Kim, Y.; Yeom, H. R.; Kim, J. Y.; Yang, C. High-efficiency Polymer Solar Cells with A Cost-effective Quinoxaline Polymer through Nanoscale Morphology Control Induced by Practical Processing Additives. *Energy Environ. Sci.* **2013**, *6*, 1909−1916.
(29) Wang, E.; Bergqvist, J.; Vandewal, K.; Ma, Z.; Hou, L.; Lundin, A.; Himmelberger, S.; Salleo, A.; Müller, C.; Inganäs, O.; Zhang, F.; Andersson, M. R. Conformational Disorder Enhances Solubility and Photovoltaic Performance of a Thiophene−Quinoxaline Copolymer. *Adv. Energy Mater.* **2013**, *3*, 806−814.
(30) Andersson, L. M. Charge Transport and Energetic Disorder in Polymer:fullerene Blends. *Org. Electron.* **2011**, *12*, 300−305.
(31) Zhou, C.; Liang, Y.; Liu, F.; Sun, C.; Huang, X.; Xie, Z.; Huang, F.; Roncali, J.; Russell, T. P.; Cao, Y. Chain Length Dependence of the Photovoltaic Properties of Monodisperse Donor−Acceptor Oligomers as Model Compounds of Polydisperse Low Band Gap Polymers. *Adv. Funct. Mater.* **2014**, *24*, 7538−7547.
(32) Liu, X.; Sun, Y.; Perez, L. A.; Wen, W.; Toney, M. F.; Heeger, A. J.; Bazan, G. C. Narrow-Band-Gap Conjugated Chromophores with Extended Molecular Lengths. *J. Am. Chem. Soc.* **2012**, *134*, 20609−20612.
(33) Li, Z.; He, G.; Wan, X.; Liu, Y.; Zhou, J.; Long, G.; Zuo, Y.; Zhang, M.; Chen, Y. Solution Processable Rhodanine-Based Small Molecule Organic Photovoltaic Cells with a Power Conversion Efficiency of 6.1%. *Adv. Energy Mater.* **2012**, *2*, 74−77.
(34) Zhou, J.; Wan, X.; Liu, Y.; Zuo, Y.; Li, Z.; He, G.; Long, G.; Ni, W.; Li, C.; Su, X.; Chen, Y. Small Molecules Based on Benzo[1,2-b:4,5-b′]dithiophene Unit for High-Performance Solution-Processed Organic Solar Cells. *J. Am. Chem. Soc.* **2012**, *134*, 16345−16351.
(35) Cardona, C. M.; Li, W.; Kaifer, A. E.; Stockdale, D.; Bazan, G. C. Electrochemical Considerations for Determining Absolute Frontier Orbital Energy Levels of Conjugated Polymers for Solar Cell Applications. *Adv. Mater.* **2011**, *23*, 2367−2371.
(36) Chai, J.-D.; Head-Gordon, M. Long-range Corrected Hybrid Density Functionals with Damped Atom-atom Dispersion Corrections. *Phys. Chem. Chem. Phys.* **2008**, *10*, 6615−6620.
(37) Hedström, S.; Persson, P. Quantum Chemical Calculations of Side-Group Stacking and Electronic Properties in Thiophene−Quinoxaline Polymers. *J. Phys. Chem. C* **2012**, *116*, 26700−26706.
(38) Adamo, C.; Barone, V. Toward Reliable Density Functional Methods without Adjustable Parameters: The PBE0Model. *J. Chem. Phys.* **1999**, *110*, 6158−6170.
(39) Hedstrom, S.; Henriksson, P.; Wang, E.; Andersson, M. R.; Persson, P. Light-harvesting Capabilities of Low Band Gap Donor-acceptor Polymers. *Phys. Chem. Chem. Phys.* **2014**, *16*, 24853−24865.
(40) Zhang, G.; Musgrave, C. B. Comparison of DFT Methods for Molecular Orbital Eigenvalue Calculations. *J. Phys. Chem. A* **2007**, *111*, 1554−1561.
(41) Huang, Y.; Kramer, E. J.; Heeger, A. J.; Bazan, G. C. Bulk Heterojunction Solar Cells: Morphology and Performance Relationships. *Chem. Rev.* **2014**, *114*, 7006−7043.
(42) Li, G.; Shrotriya, V.; Huang, J.; Yao, Y.; Moriarty, T.; Emery, K.; Yang, Y. High-efficiency Solution Processable Polymer Photovoltaic Cells by Self-organization of Polymer Blends. *Nat. Mater.* **2005**, *4*, 864−868.
(43) Brabec, C. J.; Heeney, M.; McCulloch, I.; Nelson, J. Influence of Blend Microstructure on Bulk Heterojunction Organic Photovoltaic Performance. *Chem. Soc. Rev.* **2011**, *40*, 1185−1199.
(44) Hexemer, A.; Bras, W.; Glossinger, J.; Schaible, E.; Gann, E.; Kirian, R.; MacDowell, A.; Church, M.; Rude, B.; Padmore, H. A SAXS/WAXS/GISAXS Beamline with Multilayer Monochromator. *J. Phys.: Conf. Ser.* **2010**, *247*, 012007.

DOI: 10.1021/acsami.5b09460
ACS Appl. Mater. Interfaces XXXX, XXX, XXX−XXX